3-2014

Neutral Nitrogen Acceptors in ZnO: The ^{67}Zn Hyperfine Interactions

Eric M. Golden [*]
Air Force Institute of Technology

S. M. Evans
West Virginia University

Larry E. Halliburton
West Virginia University

Nancy C. Giles
Air Force Institute of Technology

Neutral nitrogen acceptors in ZnO: The ^{67}Zn hyperfine interactions

E. M. Golden, S. M. Evans, L. E. Halliburton, and N. C. Giles

View Online   Export Citation   CrossMark

ARTICLES YOU MAY BE INTERESTED IN

Neutral nitrogen acceptors in ZnO: The ^{67}Zn hyperfine interactions

E. M. Golden,[1] S. M. Evans,[2] L. E. Halliburton,[2] and N. C. Giles[1,a)]

[1]*Department of Engineering Physics, Air Force Institute of Technology, Wright-Patterson Air Force Base, Ohio 45433, USA*
[2]*Department of Physics, West Virginia University, Morgantown, West Virginia 26506, USA*

Electron paramagnetic resonance (EPR) is used to characterize the ^{67}Zn hyperfine interactions associated with neutral nitrogen acceptors in zinc oxide. Data are obtained from an *n*-type bulk crystal grown by the seeded chemical vapor transport method. Singly ionized nitrogen acceptors (N$^-$) initially present in the crystal are converted to their paramagnetic neutral charge state (N^0) during exposure at low temperature to 442 or 633 nm laser light. The EPR signals from these N^0 acceptors are best observed near 5 K. Nitrogen substitutes for oxygen ions and has four nearest-neighbor cations. The zinc ion along the [0001] direction is referred to as an axial neighbor and the three equivalent zinc ions in the basal plane are referred to as nonaxial neighbors. For axial neighbors, the ^{67}Zn hyperfine parameters are A$_\parallel$ = 37.0 MHz and A$_\perp$ = 8.4 MHz with the unique direction being [0001]. For nonaxial neighbors, the ^{67}Zn parameters are A$_1$ = 14.5 MHz, A$_2$ = 18.3 MHz, and A$_3$ = 20.5 MHz with A$_3$ along a [10$\bar{1}$0] direction (i.e., in the basal plane toward the nitrogen) and A$_2$ along the [0001] direction. These ^{67}Zn results and the related ^{14}N hyperfine parameters provide information about the distribution of unpaired spin density at substitutional neutral nitrogen acceptors in ZnO. © 2014 AIP Publishing LLC. [http://dx.doi.org/10.1063/1.4867736]

I. INTRODUCTION

Nitrogen substitutes for oxygen in ZnO and forms an optically active acceptor. Electron paramagnetic resonance (EPR) provides a sensitive and high-resolution method to monitor these acceptors. In *n*-type material, nitrogen acceptors are normally in the singly ionized charge state with no unpaired spins and no EPR signal. However, when these samples are illuminated at low temperature with near-band-edge laser light, a portion of the singly ionized nitrogen acceptors are converted to the neutral charge state, and thus become paramagnetic. Using bulk *n*-type ZnO crystals, Carlos *et al.*[1] and Garces *et al.*[2] were the first to identify the photoinduced EPR spectrum from neutral nitrogen acceptors. As expected, the spectrum is uniquely distinguished by a well-resolved three-line ^{14}N hyperfine pattern. This neutral-nitrogen-acceptor spectrum is also seen in powder and polycrystalline ZnO.[3,4] Recent investigations[4–6] show that prominent forbidden lines appearing in the EPR spectrum are due to a ^{14}N nuclear electric quadrupole interaction.

The question as to whether an isolated nitrogen is a deep or shallow acceptor in ZnO has received considerable attention in recent years. Advanced first-principles calculations[7–10] have suggested that nitrogen is a deep acceptor with an ionization energy approaching 1.3 eV. On the experimental side, the wavelength dependence of the photo-conversion of singly ionized nitrogen acceptors to the neutral charge state has an onset near 2.0 eV and provides evidence that nitrogen is a deep acceptor in ZnO.[5] Additional support for the deep acceptor model of nitrogen comes from the observation of a broad photoluminescence band peaking near 730 nm in nitrogen-doped

bulk crystals.[11] In contrast, a donor-acceptor pair (DAP) peak is observed in photoluminescence studies of nitrogen-doped ZnO epilayers and is assigned to a shallow donor to shallow acceptor transition with an acceptor binding energy of around 160 meV and a donor binding energy near 60 meV.[12] It is not known if the participating shallow acceptor is an isolated nitrogen or a larger complex involving one or more nitrogen ions. The important point, however, is that these DAP results[12] show shallow acceptors are formed in ZnO by nitrogen doping. The conflicting nature of the reports thus far suggests a need for additional fundamental studies of nitrogen-doped ZnO.

In the present paper, EPR is used to investigate the ^{67}Zn hyperfine interactions associated with the neutral nitrogen acceptor in ZnO. Sets of less intense lines are observed around each of the primary ^{14}N lines in the photoinduced spectra taken at 5 K (using 442 or 633 nm laser light). They are assigned to axial and nonaxial ^{67}Zn nearest-neighbors. Principal values and principal-axis directions of the ^{67}Zn hyperfine matrices are obtained from the angular dependence of the EPR spectra. These spin-Hamiltonian parameters provide information about the distribution of the unpaired spin at the zinc neighbors. Comparing the experimentally determined ^{67}Zn and ^{14}N hyperfine parameters with values predicted by density-functional-theory (DFT) calculations is expected to provide a check on the validity of the deep-acceptor model of nitrogen substituting for oxygen in ZnO with no nearby perturbations.[4,13,14]

II. EXPERIMENTAL

The bulk ZnO crystal used in the present investigation was cut from a larger boule grown at Eagle-Picher (Miami, OK) by the seeded chemical-vapor-transport method with N$_2$

---

a)Author to whom correspondence should be addressed: Electronic mail: Nancy.Giles@afit.edu

added to the gas stream. Material from this boule was used in a previous study[15] of nitrogen in ZnO. The as-grown boule appeared yellow and Hall measurements at room temperature verified that it was *n* type. In addition to the usual shallow-donor signal, EPR showed that Fe^{3+} ions were present before illumination at low temperature. Dimensions of the EPR sample were approximately $3 \times 3 \times 1 \, mm^3$. Figure 1 shows a nitrogen ion substituting for an oxygen ion in the ZnO wurtzite structure. The nitrogen has four nearest-neighbor zinc ions (one axial and three nonaxial) and twelve neighboring oxygen ions (divided into three sets of 3, 6, and 3 with the middle set of 6 slightly more distant from the nitrogen than the upper and lower sets of 3).

The EPR spectra were taken using a Bruker EMX spectrometer operating near 9.39 GHz. Magnetic field values were obtained with a proton teslameter. A Cr-doped MgO crystal was used to correct for the difference in magnetic field between the sample position and the probe tip of the teslameter (Cr^{3+} in MgO has an isotropic g value of 1.9800). The sample temperature was controlled with an Oxford Instruments helium-gas flow system. Helium-cadmium (442 nm) and helium-neon (633 nm) lasers were separately used to successfully convert the nitrogen acceptors from the singly ionized charge state to the paramagnetic neutral charge state at low temperature. The laser light "moves" electrons from the valence band or singly ionized acceptors to shallow donors and deeper Fe donors, where they remain stably trapped as long as the temperature is kept below about 100 K. From the intensities of their EPR signals, the largest concentration of neutral nitrogen acceptors photoinduced in our sample is estimated to be approximately $8.0 \times 10^{15} \, cm^{-3}$.

III. RESULTS

Figure 2 shows the well resolved and unique sets of three lines that characterize the EPR spectra from isolated neutral nitrogen acceptors in ZnO.[1–6] The magnetic field is along the [0001] direction (i.e., the *c* axis) in Fig. 2(a) and is in the basal plane along the [10$\bar{1}$0] direction in Fig. 2(b). Both spectra were taken at 5 K after an exposure at this
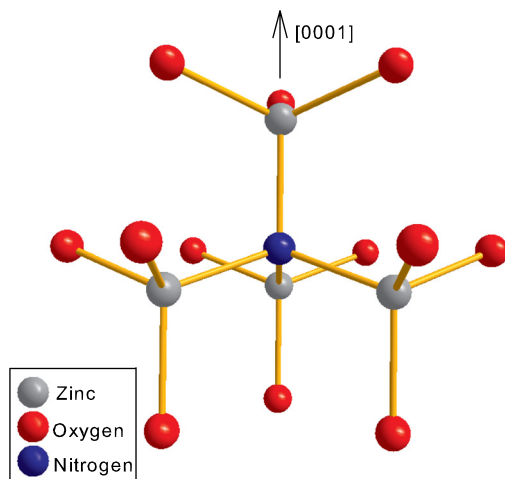

FIG. 1. A schematic representation of the ZnO wurtzite lattice as seen along the [10$\bar{1}$0] direction. A nitrogen substitutes for an oxygen and has four neighboring zinc ions and twelve neighboring oxygen ions.
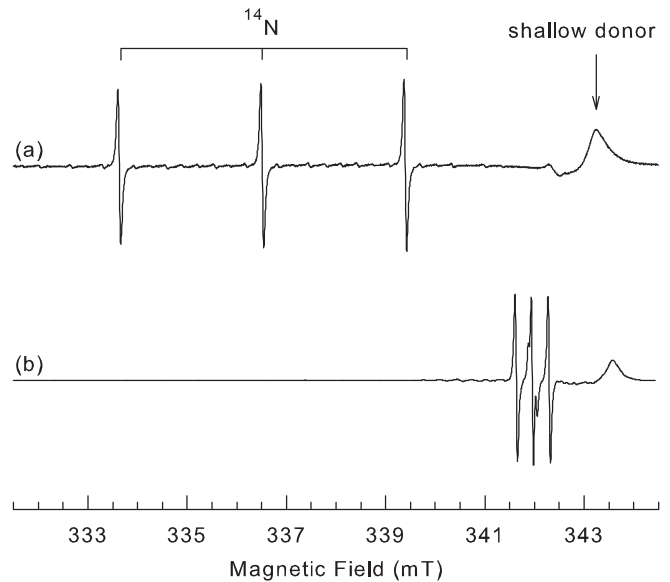

FIG. 2. Photoinduced EPR from the neutral nitrogen acceptor. These spectra were taken at 5 K after illumination at this temperature with 442 nm laser light. The microwave frequency was 9.3958 GHz. (a) The magnetic field is in the [0001] direction. (b) The magnetic field is in the basal plane along the [10$\bar{1}$0] direction.

temperature to 442 nm laser light (633 nm laser light produced the same spectra). At temperatures above approximately 9 K, these EPR lines broaden beyond recognition because of short spin-lattice relaxation times. The set of three lines is the result of a hyperfine interaction between the unpaired spin (S = 1/2) and a ^{14}N nucleus (99.6% abundant with I = 1). The angular dependence of the EPR spectrum is described by the following spin Hamiltonian with $\mathbf{I^N}$ being the nuclear spin of nitrogen:

$$\mathbf{H} = \beta \mathbf{S} \cdot \mathbf{g} \cdot \mathbf{B} + \mathbf{I^N} \cdot \mathbf{A^N} \cdot \mathbf{S} + \mathbf{I^N} \cdot \mathbf{Q^N} \cdot \mathbf{I^N} - g_N \beta_N \mathbf{I^N} \cdot \mathbf{B}. \quad (1)$$

Parameters for the *g* matrix, the ^{14}N hyperfine matrix ($\mathbf{A^N}$), and the nuclear electric quadrupole matrix ($\mathbf{Q^N}$) have been independently determined by several groups.[4–6] The values reported by Evans[6] are listed in Table I. Giamello *et al.*[4] determined that the signs of $A_\parallel$ and $A_\perp$ for the ^{14}N nucleus are opposite. We assign a positive sign to $A_\parallel$ because the nuclear g factor for ^{14}N is positive. The $\mathbf{Q^N}$ matrix is traceless with $Q_1 = Q_2 = -P$, and $Q_3 = 2P$. The parameter P is defined as $e^2qQ/[4I(2I-1)]$, where eq is the electric field gradient and Q is the nuclear quadrupole moment. From experiment,[5,6] the positions of forbidden lines require $A_\perp$ and Q_3 to have opposite signs.

The three matrices in Eq. (1) have axial symmetry about the *c* axis, which verifies that the unpaired spin occupies a nitrogen *p* orbital aligned along this unique direction. The EPR lines in Fig. 2(a) shift to higher field, but do not split, as the magnetic field is rotated from [0001] to the basal plane. "Forbidden transitions" arising from the ^{14}N nuclear electric quadrupole interaction begin to appear between the "allowed" lines when the magnetic field is approximately 60° away from the [0001] direction.[5] These forbidden transitions are most intense when the field is about 86° from

TABLE I. Spin-Hamiltonian parameters for the neutral nitrogen acceptor in ZnO. The **g** matrix, the ^{14}N hyperfine matrix, and the ^{14}N nuclear electric quadrupole matrix are from Ref. 6. The ^{67}Zn hyperfine matrices are from the present study. Units for the A and Q parameters are MHz.

	Principal value	Principal-axis direction
g matrix		
$g_\perp$	1.9631	
$g_\parallel$	1.9949	[0001]
A hyperfine matrix for ^{14}N		
$A_\perp$	−7.95	
$A_\parallel$	+81.26	[0001]
Q nuclear electric quadrupole matrix for ^{14}N		
Q_1	−1.475	
Q_2	−1.475	
Q_3	+2.950	[0001]
A hyperfine matrix for axial ^{67}Zn neighbors		
$|A_\perp|$	8.4	
$|A_\parallel|$	37.0	[0001]
A hyperfine matrix for nonaxial ^{67}Zn neighbors		
$|A_1|$	14.5	[$\bar{1}2\bar{1}0$]
$|A_2|$	18.3	[0001]
$|A_3|$	20.5	[$10\bar{1}0$] (toward the nitrogen)

[0001] (allowed and forbidden lines have similar intensities near this direction). Two forbidden lines are still present, but less noticeable, when the field is in the basal plane. In Fig. 2(b), these forbidden transitions can be observed on either side of the middle allowed EPR line.

Well-resolved hyperfine lines from ^{67}Zn nearest neighbors are easily observed in the EPR spectra from the neutral nitrogen acceptors. These ^{67}Zn nuclei are 4.1% abundant and have I = 5/2. Because of this low abundance, the ^{67}Zn lines are much smaller than the primary ^{14}N lines in Fig. 2. Figure 3 shows these weaker lines in an EPR spectrum taken at 5 K after illuminating the sample at this temperature with 442 nm laser light. The magnetic field is along the [0001] direction and the microwave frequency is 9.3973 GHz. Compared to Fig. 2(a), the vertical scale is expanded to show the symmetrical sets of hyperfine lines. Stick diagrams above the spectrum identify the axial (red) and nonaxial (blue) ^{67}Zn lines

that surround each of the three off-scale ^{14}N lines. A nitrogen substituting for an oxygen has one axial zinc neighbor (in the [0001] direction) and three nonaxial zinc neighbors (in the basal plane); this makes the nonaxial lines in the EPR spectrum three times more intense. In Fig. 3, the separation of adjacent axial lines is 1.30 mT and the separation of adjacent nonaxial lines is 0.64 mT.

Spin-Hamiltonian parameters describing the axial and nonaxial hyperfine matrices are obtained from the angular dependence of the ^{67}Zn lines. For many directions of magnetic field, the majority of the lines are strongly overlapping and it is difficult to make specific assignments and extract useful information. Fortunately, there are angles where subsets of hyperfine lines on the low-field side of the EPR spectra can be assigned to specific transitions and used to determine precise values of the parameters. In the following analysis of the nitrogen EPR spectra, we focus on these low-field ^{67}Zn hyperfine lines.

A. Axial ^{67}Zn neighbor

In Fig. 3, there are three well-resolved axial ^{67}Zn lines in the field region below the ^{14}N line at 333.6 mT. These three hyperfine lines move closer to the ^{14}N line as the magnetic field is rotated from [0001] toward [$10\bar{1}0$] and no splitting into components is detected. The same behavior occurs when the field is rotated from [0001] toward [$2\bar{1}\bar{1}0$]. These observations require the [0001] direction to be a principal axis of the axial-neighbor ^{67}Zn hyperfine matrix and they also suggest that this matrix is very close to axial (i.e., $A_1 = A_2 = A_\perp$). A plot of the axial hyperfine lines is shown in Fig. 4 for rotation of the magnetic field from [0001] to [$10\bar{1}0$]. The solid lines represent the ^{67}Zn interactions and the dashed lines represent only the ^{14}N interaction (nonaxial ^{67}Zn lines are not plotted in Fig. 4). The set of six lines in red surround the low-field ^{14}N line, the set of six lines in green surround the middle ^{14}N line, and the set of six lines in blue surround the high-field ^{14}N line. The discrete points in Fig. 4 are experimental results.

These low-field axial ^{67}Zn lines could be accurately identified and measured only during the first 40° of rotation from [0001]. Beyond this angle, nonaxial ^{67}Zn lines begin to interfere. The axial lines extend out farther from the
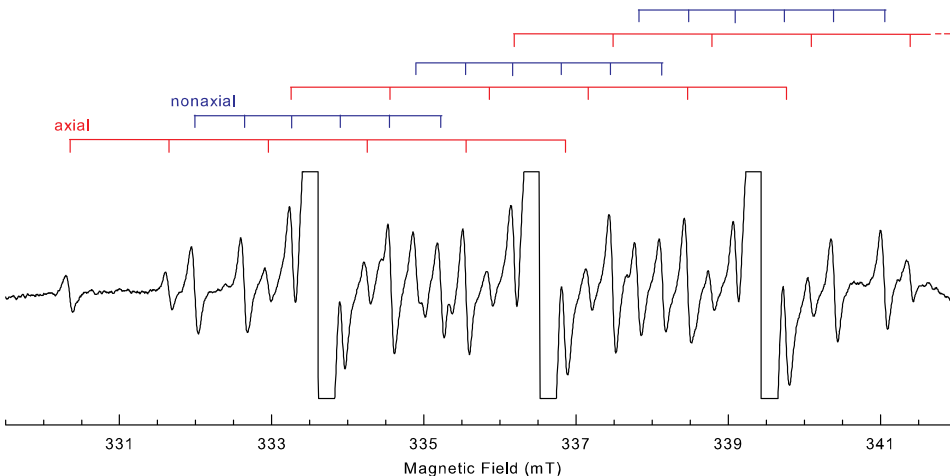

FIG. 3. ^{67}Zn hyperfine lines in the photoinduced EPR spectrum of the neutral nitrogen acceptor. This spectrum was taken at 5 K after illumination with 442 nm laser light. The magnetic field is in the [0001] direction. Stick diagrams show the axial (red) and nonaxial (blue) ^{67}Zn lines that surround each of the three large (off-scale) ^{14}N hyperfine lines.
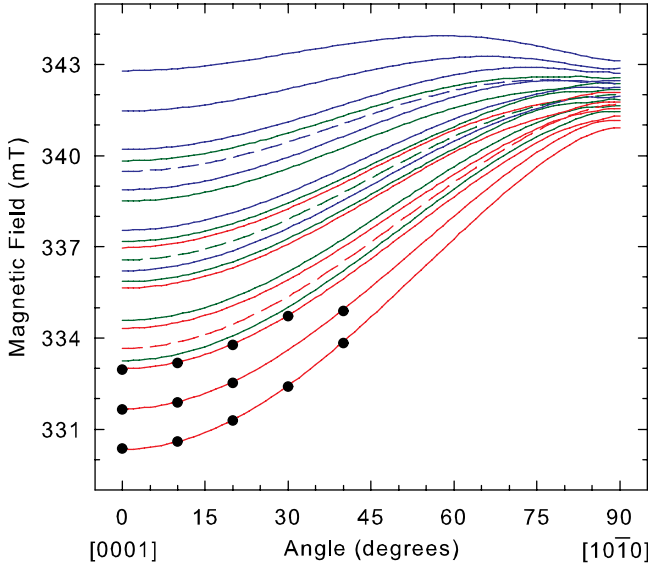
FIG. 4. Angular dependence of the axial ^{67}Zn hyperfine lines when the magnetic field rotates from the [0001] direction to the [10$\bar{1}$0] direction. The microwave frequency is 9.3974 GHz. Discrete points are experimental results and solid curves are computer-generated using the parameters in Table I.

large low-field ^{14}N line than the nonaxial lines when the magnetic field is along the [0001] direction (as seen in Fig. 3). However, as the magnetic field is rotated from [0001] toward the basal plane, this ordering reverses for angles beyond 40°. For angles greater than 40° (i.e., as the magnetic field approaches the basal plane), the nonaxial ^{67}Zn lines extend farther out from the large ^{14}N line than the axial ^{67}Zn lines. In the basal plane, the axial ^{67}Zn lines are completely obscured by the inner nonaxial lines. This interference from nonaxial lines limits the range where the axial lines can be measured, and thus accounts for the lack of data points beyond 40° in Fig. 4. Fortunately, the experimental results obtained from the first 40° of rotation are sufficient to determine the axial ^{67}Zn hyperfine parameters ($A_\parallel$ and $A_\perp$).

The spin Hamiltonian in Eq. (1) was expanded to include the following zinc-related terms:

$$+ \mathbf{I^{Zn}} \cdot \mathbf{A^{Zn}} \cdot \mathbf{S} - g_N \beta_N \mathbf{I^{Zn}} \cdot \mathbf{B}. \qquad (2)$$

The complete spin Hamiltonian with $S = 1/2$, $I^N = 1$, and $I^{Zn} = 5/2$ was then written as a 36 × 36 matrix and used in an iterative fitting routine to find the best values of the parameters describing the axial ^{67}Zn hyperfine matrix. During this process, the **g**, $\mathbf{A^N}$, and $\mathbf{Q^N}$ matrices were not varied. The 13 data points in Fig. 4 were used as input and the resulting "best-fit" values of $A_\parallel$ and $A_\perp$ are included in Table I. The relative signs of $A_\parallel$ and $A_\perp$ are not determined in our experiments. These axial ^{67}Zn parameters and the ^{14}N parameters in Table I were used to generate the solid and dashed curves in Fig. 4. The estimated uncertainties are ±0.2 MHz for $A_\parallel$ and ±2.0 MHz for $A_\perp$. A lack of experimental data for the axial nucleus at angles close to the basal plane in Fig. 4 is responsible for the larger uncertainty for $A_\perp$.

B. Nonaxial ^{67}Zn neighbors

There are also three well-resolved nonaxial ^{67}Zn lines in the field region below the ^{14}N line at 333.6 mT in Fig. 3. The lowest-field line maintains the same spacing from the ^{14}N line for the first 30° of rotation of the magnetic field away from [0001] toward [10$\bar{1}$0] and only a slight broadening, but no splitting into components, is observed. Continued rotation causes this lowest-field nonaxial ^{67}Zn line to split into two components. When the magnetic field reaches the basal plane, the two components that emerged from the original line are well separated and easily seen. Unlike the case of the axial neighbor, EPR spectra taken in the basal plane provide detailed information about the nonaxial ^{67}Zn hyperfine interactions. Figure 5 shows two of these spectra obtained at 5 K and a microwave frequency of 9.3951 GHz after illuminating the crystal with 442 nm laser light. The magnetic field is along the [10$\bar{1}$0] direction in Fig. 5(a) and along the [2$\bar{1}\bar{1}$0] direction in Fig. 5(b). Interference from the axial ^{67}Zn lines is not a problem in the basal plane because the nonaxial ^{67}Zn lines extend farther from the primary ^{14}N lines than the axial ^{67}Zn lines. Also, in the basal plane, the nonaxial ^{67}Zn hyperfine spacings are larger than the ^{14}N hyperfine spacings. This makes it easy to identify individual nonaxial lines on the low-field side of the spectra in Fig. 5 because they appear as sets of three lines that mimic the spacing of the three large primary ^{14}N lines. The lowest-field three-line sets are identified by stick diagrams in Fig. 5.

When the magnetic field is along either the [10$\bar{1}$0] or the [2$\bar{1}\bar{1}$0] direction, two of the three zinc ions in the basal plane have equivalent hyperfine interactions. Thus, there are
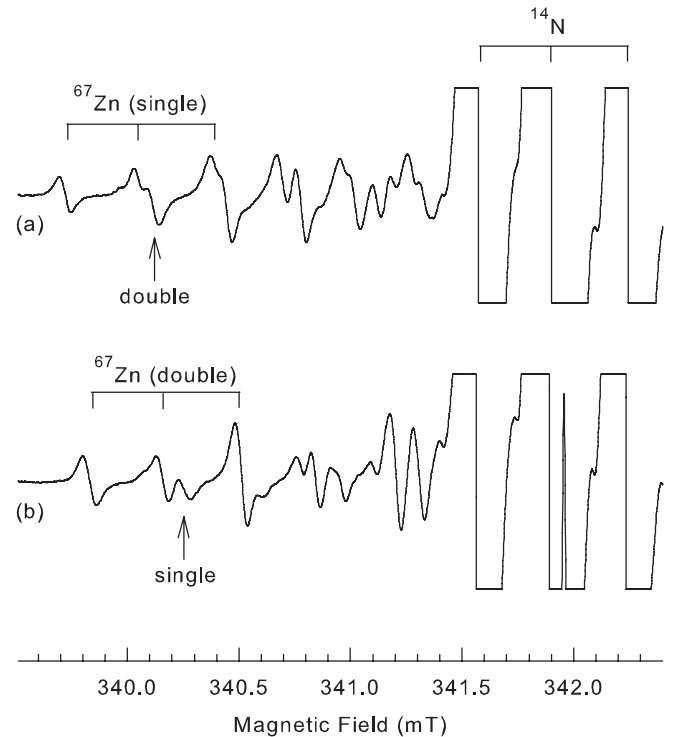

FIG. 5. Low-field ^{67}Zn hyperfine lines in the EPR spectrum when the magnetic field is in the basal plane. These data were taken at 5 K after illumination with 442 nm laser light. (a) The magnetic field is in the [10$\bar{1}$0] direction. (b) The magnetic field is in the [2$\bar{1}\bar{1}$0] direction.

two sets of nonaxial ^{67}Zn lines for these directions of field, with one set twice as intense as the other set. In Fig. 5, lines from a twice-as-intense set are labeled "double" and lines from a less-intense set are labeled "single." A less intense set of three lines (representing the interaction with one zinc nucleus) is lowest in field in Fig. 5(a) with the lowest line in this set of three located at 339.7 mT. The lowest line of the twice-as-intense set is located at 340.1 mT in Fig. 5(a). The ordering is reversed in Fig. 5(b) for the other orientation of field in the basal plane. The twice-as-intense set of three lines (representing the interaction with two equivalent zinc nuclei) is now lowest in field with the lowest line in this set of three located at 339.8 mT. The lowest line of the less-intense set is at 340.3 mT in Fig. 5(b). The experimental positions of these low-field nonaxial lines are plotted as discrete points in Fig. 6 for rotation of the magnetic field from [$2\bar{1}\bar{1}0$] to [$10\bar{1}0$].

As seen in Figs. 5(a) and 6, the lowest-field (single) nonaxial ^{67}Zn line has a turning point along the [$10\bar{1}0$] direction. This, in turn, suggests that a principal axis of the nonaxial hyperfine matrix is along this direction. Rotation of the magnetic field from the [$10\bar{1}0$] direction toward the [0001] direction provides further verification that [$10\bar{1}0$] is a principal axis direction. In this second plane of rotation, the lowest-field nonaxial ^{67}Zn line also has a turning point when the magnetic field is along the [$10\bar{1}0$] direction. Another principal axis of the nonaxial hyperfine matrix must be along the [$\bar{1}2\bar{1}0$] direction (i.e., perpendicular to the mirror plane containing the nitrogen and the nonaxial zinc neighbor). This then requires the third principal axis to be along the [0001] direction. Knowing the three principal axes allows us to extract the principal values of the nonaxial ^{67}Zn hyperfine matrix from the experimental data shown in Figs. 3 and 6. An iterative process involving the 36×36 matrix form of the spin Hamiltonian (Eqs. (1) and (2) combined) was used. Input data were 28 points from the basal plane (see Fig. 6)

and the three lowest field nonaxial lines from the [0001] spectrum (see Fig. 3). The resulting "best-fit" values of A_1, A_2, and A_3 are listed in Table I. Relative signs of these principal values are not known. The nonaxial ^{67}Zn parameters and the ^{14}N parameters in Table I were used to generate the solid curves in Fig. 6. Estimated uncertainties for A_1, A_2, and A_3 are ± 0.2 MHz.

Figure 7 is a schematic representation of the neutral nitrogen acceptor in ZnO. The axial zinc neighbor and one nonaxial zinc neighbor are shown. Two of the principal directions of the nonaxial ^{67}Zn matrix are in the basal plane with A_3 pointing toward the nitrogen. Having A_3 in the basal plane suggests that the nitrogen ion has relaxed along the [0001] direction (i.e., the nitrogen has moved away from its axial zinc neighbor to a new equilibrium position that is close to the plane containing the three nonaxial zinc neighbors). This relaxation is partially driven by the electrostatic repulsion between the "hole" on the nitrogen and the positive charge of the axial zinc ion. DFT calculations[8,10] have predicted this movement away from the axial zinc neighbor.

IV. DISCUSSION

In ZnO, a nitrogen can substitute for an oxygen and have no nearby perturbing defects. In its neutral charge state, this acceptor has an unpaired spin residing primarily in a nitrogen p orbital aligned along the [0001] direction and is easily studied with EPR. Previous magnetic resonance investigations have focused on the ^{14}N hyperfine interactions.[4,5] In the present study, complete sets of ^{67}Zn hyperfine parameters have been obtained for the one axial and the three nonaxial zinc neighbors of the neutral nitrogen acceptor. These ^{67}Zn results establish that the nitrogen is at an oxygen site and is isolated (i.e., it is not adjacent to another defect). Together, the ^{14}N and ^{67}Zn results provide information about the distribution of spin density in the ground state of this neutral defect. The ^{67}Zn hyperfine parameters, especially, address the
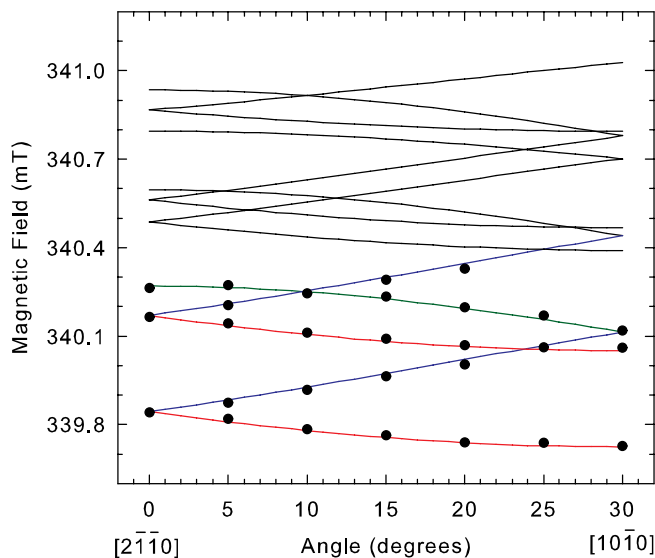

FIG. 6. Angular dependence of the nonaxial ^{67}Zn hyperfine lines when the magnetic field is rotated from the [$2\bar{1}\bar{1}0$] direction to the [$10\bar{1}0$] direction. The microwave frequency is 9.3949 GHz. Discrete points are experimental results and solid curves are computer-generated using the parameters in Table I.
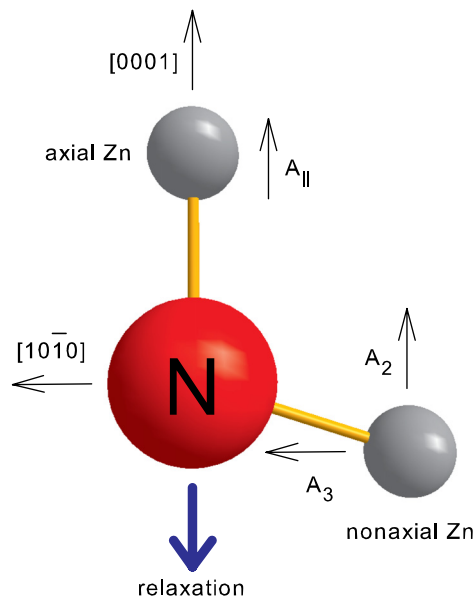

FIG. 7. Model of the neutral nitrogen acceptor in ZnO showing the directions of the principal axes for the ^{67}Zn hyperfine matrices. These three ions are in the ($\bar{1}2\bar{1}0$) plane.

delocalization of the unpaired spin and can be used as an experimental check of advanced DFT calculations.

We first discuss the primary hyperfine interaction with the central nitrogen nucleus. As described by Gallino *et al.*,[4] the ^{14}N hyperfine matrix in Table I can be separated into isotropic and anisotropic parts as follows:

$$
\mathbf{A^N} = \begin{pmatrix} -7.95 & 0 & 0 \\ 0 & -7.95 & 0 \\ 0 & 0 & +81.26 \end{pmatrix}
$$
$$
= 21.79 \begin{pmatrix} 1 & 0 & 0 \\ 0 & 1 & 0 \\ 0 & 0 & 1 \end{pmatrix}
$$
$$
+ \begin{pmatrix} -29.74 & 0 & 0 \\ 0 & -29.74 & 0 \\ 0 & 0 & +59.47 \end{pmatrix}. \qquad (3)
$$

The units in Eq. (3) are MHz. It is customary to write the **A** matrix in the following form where the parameter *a* represents the isotropic Fermi contact interaction and the parameter *b* represents the dipolar anisotropic interaction:

$$
\mathbf{A} = \begin{pmatrix} a & 0 & 0 \\ 0 & a & 0 \\ 0 & 0 & a \end{pmatrix} + \begin{pmatrix} -b & 0 & 0 \\ 0 & -b & 0 \\ 0 & 0 & 2b \end{pmatrix}. \qquad (4)
$$

This gives $a = 21.79$ MHz and $b = 29.74$ MHz for the ^{14}N nucleus. Morton and Preston,[16] and more recently Fitzpatrick *et al.*,[17] have provided results from atomic-orbital calculations that can be used to interpret experimental *a* and *b* parameters extracted from EPR hyperfine data. For a ^{14}N nucleus, Fitzpatrick *et al.*[17] predict an isotropic hyperfine value of 1540 MHz if the unpaired spin is entirely in a 2*s* orbital and an anistropic hyperfine value of 46.26 MHz (i.e., 2/5 of 115.65 MHz where 2/5 is an angular factor[16]) if the unpaired spin is entirely in a 2*p* orbital. Combining these atomic results[17] with the measured *a* and *b* values indicates that 1.4% of the unpaired spin is in a 2*s* orbital on the nitrogen and 64.3% of the unpaired spin is in a 2*p* orbital on the nitrogen. Thus, a significant portion of the unpaired spin ($\sim$65.7%) is localized on the nitrogen ion.[1,4]

The above analysis implies that approximately 34.3% of the unpaired spin is distributed on the zinc and oxygen ions neighboring the nitrogen ion. Unfortunately, hyperfine lines from the oxygen ions are not observed because the ^{17}O nuclei are only 0.038% abundant. Thus, there is no experimental information available about the amount of spin density on the oxygen ions. On the other hand, our hyperfine results for the neighboring ^{67}Zn nuclei do provide information about the unpaired spin density at the zinc ions. The isotropic parts of the ^{67}Zn matrices in Table I indicate that the unpaired spin has only a small contribution from 4*s* orbitals (less than 1%) on the zinc neighbors.[16] Larger contributions to the unpaired spin density at the zinc neighbors from the 3*d* and 4*p* orbitals are suggested by the anisotropic parts of the ^{67}Zn matrices. Interpreting these anisotropic results in terms of the 3*d* and 4*p* orbitals is, however, challenging. Depending on the choice made for the signs of the ^{67}Zn

principal values, the results of Morton and Preston[16] indicate that a significant portion of the spin density (perhaps 5% or more) may be found on each of the neighboring zinc ions. Advanced DFT quantum modeling methods appear to be the best approach to extract electronic information from these anisotropic experimental ^{67}Zn results.

It is informative to compare our ^{67}Zn hyperfine values with results from similar defects. Watts *et al.*[18] found that the axial ^{67}Zn neighbor of the neutral phosphorus acceptor in ZnSe has $A_{\parallel} = 28.8$ MHz and $A_{\perp} = 12.0$ MHz, whereas the corresponding values for the nitrogen acceptor in ZnO are 37.0 and 8.4 MHz. Hyperfine lines from ^{77}Se were also observed in the EPR spectra from the phosphorus acceptor. Another relevant example is the neutral lithium acceptor in ZnO where the "hole" is located in a 2*p* orbital of an oxygen ion adjacent to the substitutional lithium ion. Schirmer[19] suggested that the isotropic part of the hyperfine interaction for a neighboring ^{67}Zn nucleus is approximately 19.6 MHz. This is similar in magnitude to the principal values (14.5, 18.3, and 20.5 MHz) that we find for the nonaxial neighbors of the nitrogen acceptor in ZnO. A third, but quite different, example is the singly ionized oxygen vacancy in ZnO where Gonzalez *et al.*[20] determined the principal values of the ^{67}Zn hyperfine matrices for axial and nonaxial neighbors. As expected for a donor, the isotropic parts of these hyperfine matrices for the oxygen vacancy are larger than the corresponding values for the nitrogen acceptor. At the same time, the anisotropic contributions to the ^{67}Zn hyperfine matrices of the oxygen vacancy are smaller than those observed for the nitrogen acceptor.

V. SUMMARY

Resolved ^{67}Zn hyperfine structure is observed in the EPR spectra of the neutral nitrogen acceptor. The data were taken near 5 K after illuminating an *n*-type bulk ZnO crystal with 442 or 633 nm laser light. Angular studies provide the principal values and principal axes of the hyperfine matrices for the axial and nonaxial nearest-neighbor zinc ions. The directions of the nonaxial principal axes suggest that the nitrogen relaxes away from the axial zinc neighbor and into the plane of the three nonaxial zinc neighbors. When combined with the ^{14}N hyperfine results, these ^{67}Zn parameters provide a more complete description of the distribution of unpaired spin density at the neutral nitrogen acceptor in ZnO. They may also be used to check the validity of DFT calculations for this important acceptor.

[1]W. E. Carlos, E. R. Glaser, and D. C. Look, Physica B **308–310**, 976 (2001).
[2]N. Y. Garces, N. C. Giles, L. E. Halliburton, G. Cantwell, D. B. Eason, D. C. Reynolds, and D. C. Look, Appl. Phys. Lett. **80**, 1334 (2002).

[3]D. Pfisterer, J. Sann, D. M. Hofmann, M. Plana, A. Neumann, M. Lerch, and B. K. Meyer, Phys. Status Solidi B **243**, R1 (2006).

[4]F. Gallino, C. Di Valentin, G. Pacchioni, M. Chiesa, and E. Giamello, J. Mater. Chem. **20**, 689 (2010).

[5]J. E. Stehr, D. M. Hofmann, and B. K. Meyer, J. Appl. Phys. **112**, 103511 (2012).

[6]S. M. Evans, "Identification and characterization of point defects in aluminum nitride and zinc oxide crystals," Ph.D. Dissertation, West Virginia University, Morgantown, WV, 2008.

[7]J. L. Lyons, A. Janotti, and C. G. Van de Walle, Appl. Phys. Lett. **95**, 252105 (2009).

[8]S. Lany and A. Zunger, Phys. Rev. B **81**, 205209 (2010).

[9]A. Boonchun and W. R. L. Lambrecht, Phys. Status Solidi B **250**, 2091 (2013).

[10]S. Sakong, J. Gutjahr, and P. Kratzer, J. Chem. Phys. **138**, 234702 (2013).

[11]M. C. Tarun, M. Zafar Iqbal, and M. D. McCluskey, AIP Adv. **1**, 022105 (2011).

[12]S. Lautenschlaeger, S. Eisermann, G. Haas, E. A. Zolnowski, M. N. Hofmann, A. Laufer, M. Pinnisch, B. K. Meyer, M. R. Wagner, J. S. Reparaz, G. Callsen, A. Hoffmann, A. Chernikov, S. Chatterjee, V. Bornwasser, and M. Koch, Phys. Rev. B **85**, 235204 (2012).

[13]M. S. Bahramy, M. H. F. Sluiter, and Y. Kawazoe, Phys. Rev. B **73**, 045111 (2006).

[14]E. D. Hedegard, J. Kongsted, and S. P. A. Sauer, J. Chem. Theory Comput. **7**, 4077 (2011).

[15]N. Y. Garces, L. Wang, N. C. Giles, L. E. Halliburton, G. Cantwell, and D. B. Eason, J. Appl. Phys. **94**, 519 (2003).

[16]J. R. Morton and K. F. Preston, J. Magn. Reson. **30**, 577 (1978).

[17]J. A. J. Fitzpatrick, F. R. Manby, and C. M. Western, J. Chem. Phys. **122**, 084312 (2005).

[18]R. K. Watts, W. C. Holton, and M. de Wit, Phys. Rev. B **3**, 404 (1971).

[19]O. F. Schirmer, J. Phys. Chem. Solids **29**, 1407 (1968).

[20]C. Gonzalez, D. Galland, and A. Herve, Phys. Status Solidi B **72**, 309 (1975).